Journal of Computer-Aided Molecular Design (2018) 32:459–471
https://doi.org/10.1007/s10822-018-0099-9

An insight to the molecular interactions of the FDA approved HIV PR drugs against L38L↑N↑L PR mutant

Zainab K. Sanusi[1] · Thavendran Govender[1] · Glenn E. M. Maguire[1,2] · Sibusiso B. Maseko[1] · Johnson Lin[3] · Hendrik G. Kruger[1] · Bahareh Honarparvar[1]

Received: 29 August 2017 / Accepted: 16 January 2018 / Published online: 3 February 2018

Abstract

The aspartate protease of the human immune deficiency type-1 virus (HIV-1) has become a crucial antiviral target in which many useful antiretroviral inhibitors have been developed. However, it seems the emergence of new HIV-1 PR mutations enhances drug resistance, hence, the available FDA approved drugs show less activity towards the protease. A mutation and insertion designated L38L↑N↑L PR was recently reported from subtype of C-SA HIV-1. An integrated two-layered ONIOM (QM:MM) method was employed in this study to examine the binding affinities of the nine HIV PR inhibitors against this mutant. The computed binding free energies as well as experimental data revealed a reduced inhibitory activity towards the L38L↑N↑L PR in comparison with subtype C-SA HIV-1 PR. This observation suggests that the insertion and mutations significantly affect the binding affinities or characteristics of the HIV PIs and/or parent PR. The same trend for the computational binding free energies was observed for eight of the nine inhibitors with respect to the experimental binding free energies. The outcome of this study shows that ONIOM method can be used as a reliable computational approach to rationalize lead compounds against specific targets. The nature of the intermolecular interactions in terms of the host–guest hydrogen bond interactions is discussed using the atoms in molecules (AIM) analysis. Natural bond orbital analysis was also used to determine the extent of charge transfer between the QM region of the L38L↑N↑L PR enzyme and FDA approved drugs. AIM analysis showed that the interaction between the QM region of the L38L↑N↑L PR and FDA approved drugs are electrostatic dominant, the bond stability computed from the NBO analysis supports the results from the AIM application. Future studies will focus on the improvement of the computational model by considering explicit water molecules in the active pocket. We believe that this approach has the potential to provide information that will aid in the design of much improved HIV-1 PR antiviral drugs.

Keywords L38L↑N↑L PR · HIV PR inhibitors · Inhibitor–enzyme interactions · Our own N-layered Integrated molecular orbital and molecular mechanics (ONIOM) · Binding free energies · Atoms in molecules (AIM) · Natural bond orbital (NBO)

Introduction

HIV-1 belongs to the group of retroviruses known as lentiviruses and has a di-symmetric aspartyl protease [1–4]. This protein is one of the most recognized and researched enzymes regarding its function and structure and these efforts have paved the way for the development of effective inhibitors [3, 5]. The protease (PR) is normally composed of two identical 99-amino acids in each monomer, in which the amino and carboxyl termini combine at the β-sheet dimer interface and form a hydrophobic binding site with two aspartic acids (ASP25/25′) at the active site [6–8].

Electronic supplementary material The online version of this article (https://doi.org/10.1007/s10822-018-0099-9) contains supplementary material, which is available to authorized users.

✉ Hendrik G. Kruger
kruger@ukzn.ac.za

✉ Bahareh Honarparvar
Honarparvar@ukzn.ac.za; baha.honarparvar@gmail.com

[1] Catalysis and Peptide Research Unit, School of Health Sciences, University of KwaZulu-Natal, Durban 4001, South Africa

[2] School of Chemistry and Physics, University of KwaZulu-Natal, Durban 4001, South Africa

[3] School of Life Sciences, University of KwaZulu-Natal, Durban 4001, South Africa

The HIV-1 PR functions by cleaving the gag and pol viral polypeptides into building blocks for protein synthesis to create a mature functional HIV virus [9–12]. HIV-1 protease is one of the principal target for HIV/AIDS drug inhibitors since the PR is essential for the development of viable progeny [1, 13–15]. The presence of these inhibitors significantly retracts the function of the PR, preventing the virus from maturing in the affected individual [10, 16]. The nine HIV-1 protease antiretroviral drugs approved by the FDA were developed for subtype B which is the more common strain found in North America, Western Europe and Australia. These drugs exhibit weaker activities against subtype C and A found predominantly in sub-Sahara Africa and India [17–19].

The development of HIV PR resistance due to mutations causes enormous hindrance in attaining long-term suppression of HIV replication in patients receiving anti-retroviral drugs [20]. Alterations in HIV PR were first investigated by Hodge et al. [21]. They argued the actual importance of the observed changes is unclear since the mutations repeatedly occur with extra mutations in the protease and also in the viral genome [21]. Accessing the growth properties of the mutations and effect of the alteration in the viral genome will help in understanding the function of the protease gene [22, 23]. Hence, improvements can only be made on the newly designed drugs since much cannot be done on the genetic source of drug resistance [24–27].

Our research group reported inhibitor synthesis for C-SA HIV protease and computational methods to rationalize observed experimental data [28–35]. A computational model to calculate the binding free energies of HIV PR inhibitors against subtype B and C-SA PR utilizing molecular dynamics (MM-GBSA) was developed by our group [36–38]. These computational binding free energies revealed that the absolute experimental values for the binding free energies versus theoretical values differ due to the available parameterization implemented in the theoretical model, which is an approximation of experimental data [39]. However, the calculated results still follow a similar trend with the experimental data for subtype B [36, 37].

We have also recently investigated an ONIOM [40, 41] model to calculate the binding free energies of the nine FDA HIV-1 protease inhibitors against subtype B and C-SA PR [42], these were compared with the experimental binding free energies [43]. It was observed that the obtained theoretical data follow a satisfactory trend with the reported experimental data for this subtype. However, the applied model for the C-SA HIV PR revealed limitations [42].

Several other studies have utilized the ONIOM model for calculating binding energies of wild-type HIV PR-1 with selected commercial inhibitors [44–46]. In all cases, the catalytic aspartate residues were treated at a high-level theory (DFT), and the rest of the system was modelled with MM. The choice of protonation state for the catalytic HIV PR aspartates (Asp 25/25′) for ONIOM calculations has been studied extensively in literature [28, 33, 47–49]. The p*K*a of one of the catalytic aspartate increases to 5.2 [3] when bound to the inhibitor and the corresponding value is 4.5 [50] when unbound [51]. This implies that one of the two catalytic Asp groups should be protonated for binding studies, while the other Asp is unprotonated [30].

The C-SA HIV-1 protease mutant consists of two extra amino acids, resulting in a C-SA PR mutant (L38L↑N↑L) [52] with 101-amino acid residues in each monomer. The arrow (↑) before the amino acids shows that asparagine and leucine are inserted at position 38 respectively. In addition, the following five mutations have also occurred in the protease E35D, I36G, N37S, M46L and D60E [52].

This variant was found in a patient that was drug-naïve to commercially accessible HIV protease drugs but reacted positively to the following reverse transcriptase inhibitors (RTIs): d4t (stavudine), 3TC (lamivudine), and efavirenz [52] (Fig. 1).

In the present study, a hybrid ONIOM model was applied to compute the free binding energies of the nine FDA approved HIV-1 protease inhibitors towards a new HIV subtype C-SA PR mutant that also experience two insertions. To provide deeper insight on the intermolecular interactions between the QM region of the L38L↑N↑L PR and FDA approved drugs, the atom in molecules (AIM) [53, 54], was applied to characterize the nature of the intermolecular hydrogen bonds. Natural bond orbital (NBO) [55], identified the charge transfer between the QM region of the L38L↑N↑L PR enzyme and FDA approved drugs.

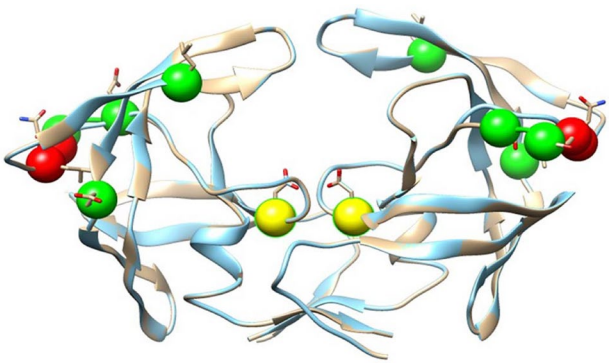

Fig. 1 Schematic representation of super-imposed subtype C-SA (blue) and mutant L38L↑N↑L PR (brown), showing the position of the mutations (E35D, I36G, N37S, M46L and D60E) in green, insertions (asparagine and leucine) are depicted in red, and Asp25/25′ in yellow

Computational methods

Homology modelling [30, 56–59] was performed to generate the three-dimensional structure for L38L↑N↑L protease by our research group as there was no single crystal X-ray structure available for the mutant. The same computational model as our recent ONIOM paper on subtype B and C-SA was utilized [42]. In this multi-layered approach, the active site was treated with a high level density functional theory [60, 61] using B3LYP [62, 63]/6-31G(d) [64, 65] basis set, while the rest of the protease was treated at a low MM level using AMBER [66] force field. Further structural analysis to estimate the mode of interactions between the ligand and L38L↑N↑L protease will be performed using the Accelrys (Discovery) Visualizer [67] and Ligplot [68] software. In addition, the AIM2000 software [69] and NBO [55] analyses were applied to measure and understand the strength and stability of the intermolecular bond interactions.

Structural preparation of inhibitor–enzyme complexes

The structures of clinically available FDA inhibitors complexed with the HIV-1 subtype B protease were taken from the Protein Data Bank (PDB). The PDB codes are as follows: 4YOA (DRV) [70], 4L1A (LPV) [71], 4EYR (RTV) [27], 3WSJ (IDV) [72], 3S56 (SQV) [73], 3S45 (APV) [73], 2PYM (NFV) [74], 4NJU (TPV) [75], 3EM4 (ATV) [76] (Figure S1).

Since the X-ray structures for L38L↑N↑L PR complexed with the FDA approved drugs have not yet been reported, structural preparation input structures for the nine drugs complexed to L38L↑N↑L PR, were performed using the same overlay method reported previously [36, 37, 42]. The 3D structures for all the inhibitor–L38L↑N↑L mutant PR complexes were generated by superimposing the corresponding subtype B HIV PR–inhibitor crystal complexes with the L38L↑N↑L PR using PyMOL [77], in order for the inhibitors to maintain the same position as in the subtype B PR. PyMOL evaluates the root mean square (RMS), which is a helpful measure of how well the inhibitor–enzyme complexes were superimposed. An optimal superimposition is considered acceptable if the RMS is less than 2 Å [78–80].

The protonation state of the L38L↑N↑L PR structure was assigned using PROPKA [81, 82] based on the p*K*a values at pH 7 as presented before [42]. This depicts that the catalytic aspartate at the active binding site in both chains Asp25 and Asp25′ are deprotonated and protonated respectively. It is notable that the carbonyl and amino terminus as well as the Asp, Gly, Arg, Lys amino acids were charged, while His is kept in its neutral form.

The structures of all inhibitor–enzyme complexes were refined afterwards by manually removing the ions and crystallographic water that are present from the protein from the PDB file using a text editor. Thereafter, protons were added to the required catalytic aspartate using Gauss View [83]. The catalytic Asp25/25′ residues and the inhibitors that constitute the smallest part of the system were considered at a high level (QM/DFT [60, 61]—Beck3LYP [62, 63]/6-31G(d) [64, 65]) and the remaining larger part of the system at low layer (MM—AMBER) [66] for subsequent ONIOM [40, 41] calculations. Details about the preparation of the ONIOM starting structures were presented before [42]. The method used follows an ONIOM mechanical embedding conformation, as the interaction between the Asp25/25′ residues along with the inhibitors (QM) and MM layer is described by the MM calculations [84].

All the 3D inhibitor–protease complex structures are created using PyMOL [77] software and are provided in supplementary material Figure S2. The ONIOM (Gaussian) input files as well as the optimized output files of all inhibitor–enzyme complexes are also provided with the supplementary material.

ONIOM binding free energies

An ONIOM [40, 85–87] computational model was used to calculate the binding free energies of the various PR inhibitors with the L38L↑N↑L PR. Preceding studies showed that the DFT level theory at the high level is the most common approach due to its popular balance of accuracy and efficiency [62, 63, 88], and B3LYP method provides good energies and are in excellent agreement with ab initio high level results [89–91]. Therefore, the geometry of the various nine FDA approved drugs complexed with the L38L↑N↑L PR were optimized using the two-layer ONIOM approach [B3LYP/6-31G(d):AMBER] QM:MM level of theory in Gaussian 09 [92] developed version. The extrapolated energy E_{ONIOM2} [93, 94] is defined as:

$$\Delta E_{ONIOM2} = \Delta E_{real,low} + \Delta E_{\mathrm{mod}\ el,high} - \Delta E_{\mathrm{mod}\ el,low} \quad (1)$$

Where ΔE_{real} is the energy of the entire (real) system and ΔE_{model} is the energies of the model system calculated at the high and low level respectively. A schematic representation of the ONIOM2 model is presented in Fig. 2.

The Gibbs binding free energies (ΔG) for the systems was achieved from frequency calculations of the optimized complexed structures using the two-layer ONIOM algorithm as discussed above. Thus, the change in free energies of the corresponding complex systems is expressed as:

$$\Delta G_{ONIOM} \approx \Delta G_{bind} = G_{complex} - G_{ligand} - G_{protein} \quad (2)$$

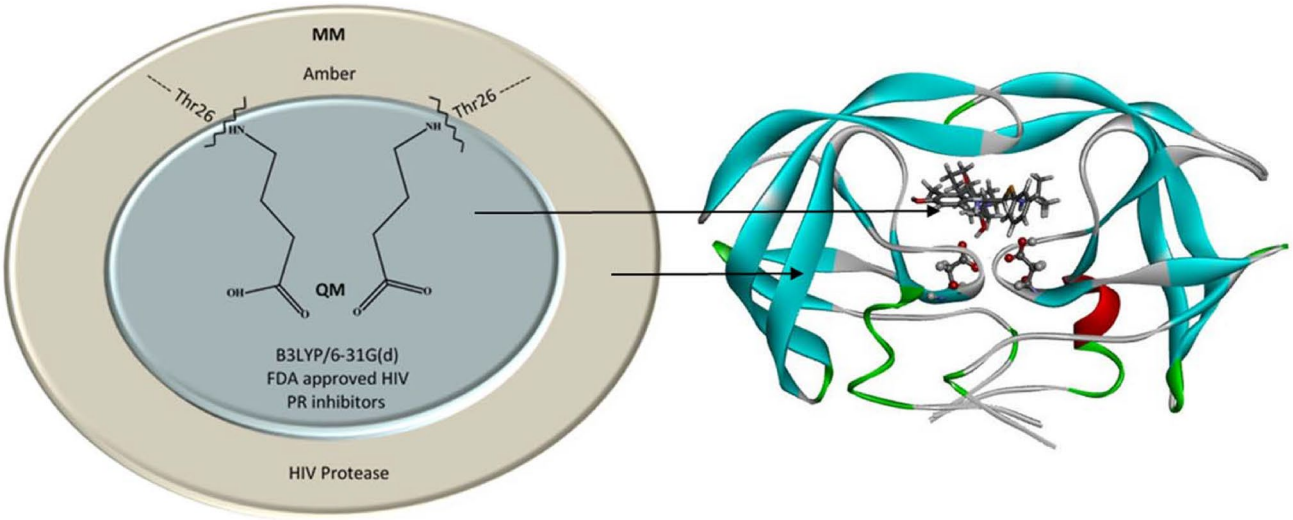

Fig. 2 Schematic diagram of the calculated two-layered ONIOM theoretical levels [B3LYP/6-31G(d): AMBER] of L38L↑N↑L PR complex with APV

Atoms in molecules (AIM) theory

The vital role of hydrogen bonding in various chemical and biological process has become an interesting area of research [95–97]. Hydrogen bond in drug design is of utmost importance due to the type of interaction that occur between the protein and their corresponding inhibitors. These intermolecular interactions not only dictate the orientation of a drug binding into its receptor but also contribute to the binding affinity [95, 98].

Bader and Popelier's theory of AIM [53, 54] is a widely-employed approach to analyse and understand hydrogen bond types. AIM theory is based on a set of proposed criteria via topological analysis including; molecular electronic charge density, $\rho(r)$, Laplacian of the electron density, $\nabla^2\rho(r)$ and the ellipticity, ε, which are calculated at the bond critical points (BCP) between the hydrogen donor atom and acceptor [99–101]. Generally, the intermolecular hydrogen bond for the electronic charge density and its Laplacian ranges between 0.002–0.040 and 0.024–0.139 a.u, respectively [101, 102]. When the value of $\nabla^2\rho(r)$ is negative at BCP, the $\rho(r)$ is locally concentrated (covalent interaction), while a positive $\nabla^2\rho(r)$ value depicts a closed shell (electrostatic) interaction and $\rho(r)$ are locally depleted [95, 103–105].

The energetic topological parameters of two bonded atoms at BCP [95, 105] can be defined as follows:

$$\frac{1}{4}\nabla^2\rho\left(r_{BCP}\right) = 2G\left(r_{BCP}\right) + V\left(r_{BCP}\right) \tag{3}$$

While,

$$H_{BCP} = G(r_{BCP}) + V(r_{BCP}) \tag{4}$$

Where H, G, and V represent the total electronic energy density, the kinetic electronic energy density and the potential electronic energy density, respectively. When the electronic charge density (H) at BCP is positive, it indicates an electrostatic interaction and its negative value depicts a covalent interaction [106, 107].

The bond ellipticity, ε is used for measuring the stability of two bonded atoms at BCP, hence, a low ellipticity value shows a more stable bond [95, 101]. This can be defined as follows [108]:

$$\varepsilon = \left(\frac{\lambda_1}{\lambda_2} - 1\right) \tag{5}$$

Where λ_1 and λ_2 denotes the two negative curvatures of the density at the BCP with respect to the X and Y principal axes.

Natural bond orbital (NBO) theory

The NBO analysis [109] provides a robust mathematical method to investigate charge transfer between hydrogen bond atoms through a set of filled Lewis and unfilled non-Lewis localized structural orbitals [110–112]. The delocalization strength (stabilization energy) is $E^{(2)}$ estimated by the second-order perturbation between a proton donor (i) and receptor (j) and is simply represented by the following equation. [95, 99, 101]:

$$E^{(2)} = \Delta E_{ij} = q_i \frac{F(i,j)^2}{e_j - e_i} \tag{6}$$

Where q_i is the occupancy number of the donor orbital, e_j and e_i are orbital energies (diagonal elements), and $F(i, j)^2$ is the off-diagonal elements of Fock matrix.

Results and discussion

To ascertain the efficiency of the FDA approved drugs against this subtype, the binding free energy calculations were performed on all the inhibitor–protease complexes with the ONIOM computational model. The average RMS values of the aligned inhibitor–L38L↑N↑L PR complex is 0.7 Å, which indicates that the complexes were correctly superimposed [78–80]. The calculated results for L38L↑N↑L PR were ranked with the experimental data (that is yet to be published), and also with our previously reported computational data for C-SA HIV PR [42] (Table 1). As it is expected and described earlier, the parameterization available in theoretical models which is an approximate of experimental data creates a considerable difference between the experimental values and theoretical values [39]. Likewise, the same difference with respect to the experimental data was also observed in our calculated results using the two-layer ONIOM model, however, the observed trend in the theoretical and experimental data are similar and informative.

The experimental results of the FDA approved drugs exhibit reduced binding free energies for the L38L↑N↑L PR mutant compared to the subtype C-SA HIV PR. Only APV possesses a reasonable binding affinity for the mutant protease in comparison to the rest of the inhibitors.

The trends of the calculated binding free energies for the FDA drugs towards C-SA HIV PR has been discussed in our previous work [42]. Here, the ONIOM (B3LYP/6-31G(d): AMBER) binding free energies of L38L↑N↑L PR demonstrate the same general trend as the experimental Gibb's free energy data but exhibit reduced theoretical binding affinities compared to subtype C-SA PR (Table 1). However, there were two exemptions (outliers); TPV shows much better binding free energy (− 61.2 kcal/mol) than other drugs complexed to the mutant enzyme. Although NFV exhibits the weakest binding affinity in both experimental and theoretical results for L38L↑N↑ L PR, the computed result appears significantly smaller than the other inhibitors (Table 1).

As it was argued in our previous study [42], the reason for these can potentially be attributed to the simplified computational model (the omission of water in the active site of the protease), rendering the model less accurate and this possibility will be interrogated further.

The insertions and mutations of amino acids residues is expected to change the structure of the mutant PR having an impact on the binding interactions between the inhibitors and the protease. Hence, detailed hydrogen bond interactions of the inhibitor–enzyme complexes were measured using Accelrys (Discovery) Visualizer [67]. The change in hydrogen bond distances were measured between both catalytic aspartates Asp25/25′ in the binding site and the hydroxyl group of the FDA approved inhibitors before and after optimization (Fig. 3). In all cases, the hydroxyl group of the inhibitors form similar hydrogen bond interactions with the Asp25/25′ of L38L↑N↑L PR (Figure S3, supplementary material). For the inhibitors exhibiting slightly better binding affinities with the L38L↑N↑L PR (APV, RTV, IDV and LPV), a large reduction in the average hydrogen bond distance 0.7 Å was observed after optimization. While inhibitors with weaker binding affinities (SQV, DRV, and

Table 1 The binding free energies[a] (kcal/mol) for FDA HIV PIs against C-SA and L38L↑N↑L PRs [reported experimental results [44] and calculated ONIOM (B3LYP/6-31G(d):AMBER) results]

Inhibitors	ΔG_{bind} (Exp)[b] C-SA	ΔG_{bind} (Exp)[b] L38L↑N↑L	ΔG_{bind} (Calc)[c] C-SA	ΔG_{bind} (Calc)[d] L38L↑N↑L
APV	− 13.9	− 13.1	− 69.0	− 56.9
RTV	− 13.9	− 12.9	− 62.9	− 56.4
IDV	− 14.0	− 12.1	− 64.0	− 52.1
LPV	− 13.2	− 11.6	− 56.5	− 51.8
SQV	− 13.4	− 10.1	− 57.1	− 45.8
DRV	− 13.8	− 9.88	− 62.8	− 43.9
ATV	− 14.4	− 9.69	− 66.9	− 43.3
TPV	− 13.2	− 9.47	− 78.9	− 61.2
NFV	− 13.5	− 9.38	− 38.6	− 24.8

The ONIOM (Gaussian) input files as well as the optimized output files of all inhibitor–enzyme complexes are also provided with the supplementary material

[a]HIV PR inhibitors with respect to their binding energies

[b]Experimental data for wildtype C-SA HIV PR and L38L↑N↑L PR carried out by our group respectively [44]

[c]Calculated binding energies of wild type C-SA HIV PR previously reported by our group [43]

[d]Calculated binding energies for L38L↑N↑L PR

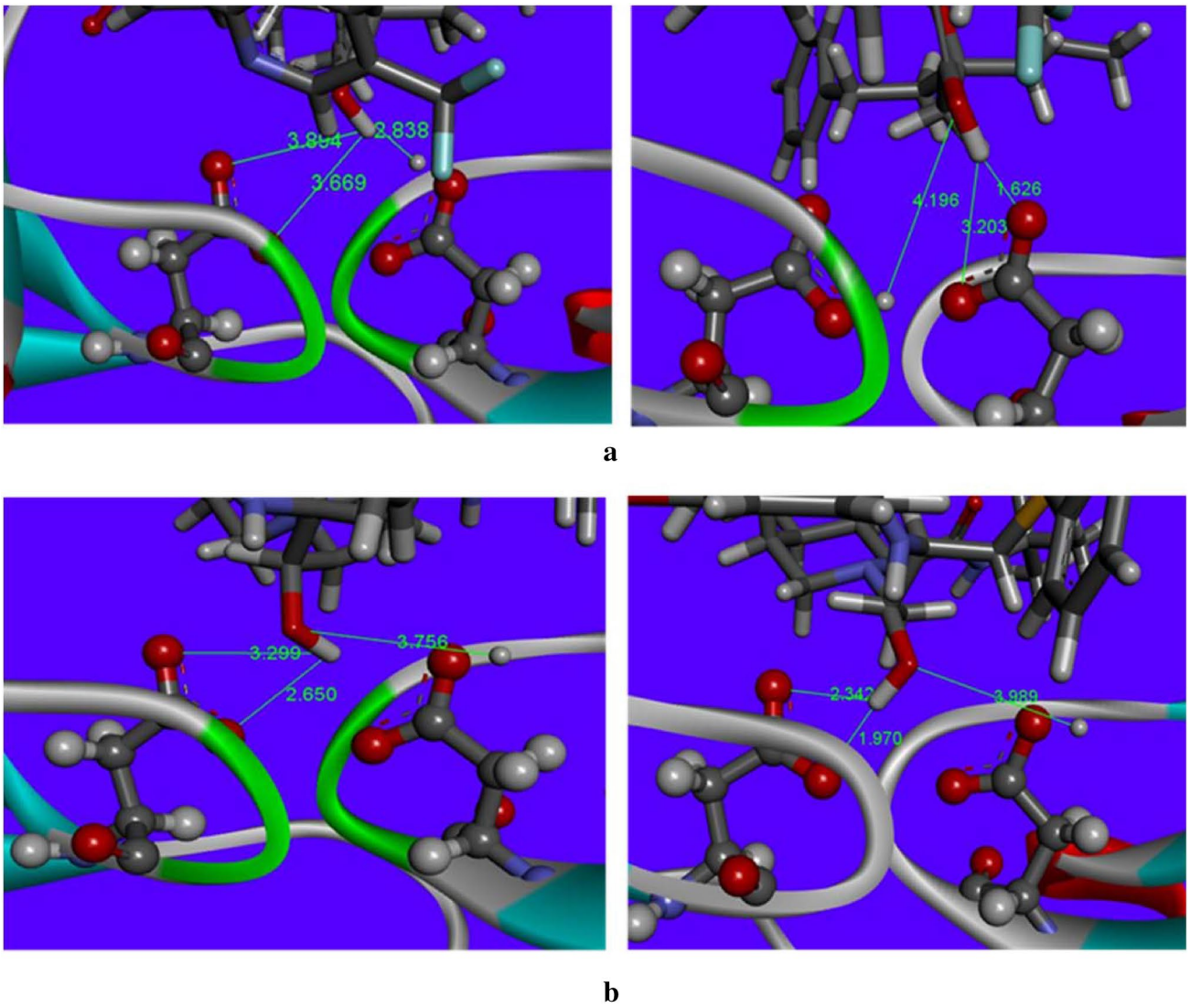

Fig. 3 Hydrogen bond distances between the hydroxyl groups of TPV and NFV drugs with the catalytic ASP25 and ASP25′ residues of **a** L38L↑N↑L——TPV PR, **b** L38L↑N↑L——NFV PR before and after optimization. Detailed comparative plots for all inhibitor–enzyme complexes are provided in supporting information Fig S3. [The ONIOM (Gaussian) input files as well as the optimized output files of all inhibitor——enzyme complexes are also provided with the supplementary material]

ATV) revealed a smaller reduction of the average hydrogen bond distance 0.1 Å.

For the outliers; TPV and NFV, a comparison of the hydrogen bond distances (Fig. 3) reveals that TPV (1.6 Å; − 61.2 kcal/mol) has a stronger HB interaction than NFV (1.9 Å; − 24.8 kcal/mol), explaining the difference in theoretical binding free energies for these two outliers.

In an attempt to further understand the binding environment within the L38L↑N↑L PR, electrostatic and hydrogen bond interactions were plotted for all inhibitor–enzyme complexes (Figure S4 in the supplementary material) with Ligplot [68]. The two exemptions; TPV and NFV are shown in Fig. 4. The plot for TPV reveals hydrogen bond and electrostatic interactions between the inhibitor and other side chain residues (NH–OH, NH–NH) in the protease, which most likely contribute to the improved binding calculation result. For NFV hydrogen bond interactions occur with the catalytic aspartates and one side chain (mainly OH–OH) resulting in weaker binding affinity.

As previously discussed, the calculated binding free energies (ΔG) for the various FDA approved inhibitors complex with L38L↑N↑L PR follow the same trend with the corresponding experimental data (Table 1), except for TPV and NFV. The thermochemical properties can be used to rationalize these outliers, since ΔG is a function of both enthalpy (ΔH) and entropy (ΔS). The calculated energies of the various drugs complexed with L38L↑N↑L PR are depicted in Table 2.

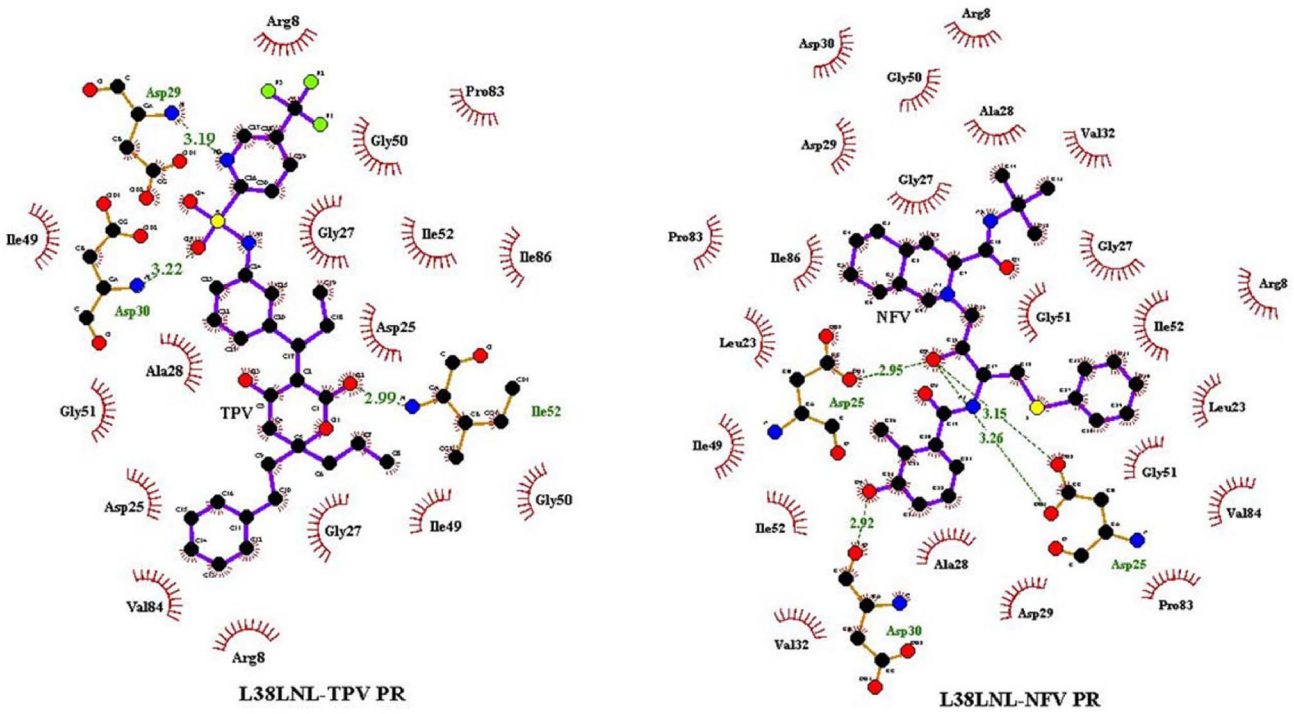

Fig. 4 Electrostatic and hydrogen bond interactions plot of L38L↑N↑L PR complexed with TPV and NPV. The plot were created after optimization of each complex system using Ligplot [1]. Detailed plots showing the electrostatic and hydrogen bond interactions are provided in supporting information Figure S4. [The ONIOM (Gaussian) input files as well as the optimized output files of all inhibitor–enzyme complexes are also provided with the supplementary material]

Table 2 The binding free energies, enthalpies and entropy of the various FDA approved HIV PIs against L38L↑N↑L PR

Inhibitors	ΔG (kcal mol^{-1})[a]	ΔH (kcal mol^{-1})	ΔS_{total} (cal mol^{-1} K^{-1})	ΔS_{trans} (cal mol^{-1} K^{-1})	ΔS_{vib} (cal mol^{-1} K^{-1})	ΔS_{rot} (cal mol^{-1} K^{-1})
APV	−56.9	−80.6	−79.4	−44.5	2.8	−37.7
RTV	−56.4	−80.5	−80.7	−45.5	4.7	−39.9
IDV	−52.1	−80.6	−95.7	−45.0	−11.3	−39.4
LPV	−51.8	−79.9	−94.1	−45.0	−10.1	−39.0
SQV	−45.8	−72.5	−89.4	−44.8	−5.2	−39.4
DRV	−43.9	−68.8	−83.4	−44.5	0.5	−39.4
ATV	−43.3	−72.0	−94.1	−44.8	−11.1	−38.2
TPV	−61.2	−82.3	−70.7	−45.0	13.6	−39.3
NFV	−24.8	−42.1	−57.9	−44.8	25.3	−38.4

HIV protease inhibitors (HIV PIs) are ranked in terms of their binding free energies (ΔG)

The ONIOM (Gaussian) input files as well as the optimized output files of all inhibitor–enzyme complexes are also provided with the supplementary material

[a]Calculated binding free energies using ONIOM for L38L↑N↑L PR from Table 1

The enthalpy contribution of TPV (ΔH −82.3 kcal/mol) is the highest of all cases, explaining why this drug binds better in theory than the other inhibitors (the enthalpy contribution is far greater than entropy to the Gibbs free binding energies). As argued before (see discussion around Fig. 3), this is most likely the result of our simplified computational model, where the interaction between the TPV hydroxyl group and the Asp25/25′ residues are over emphasized. On the other hand, NFV reveals a much-reduced enthalpy contribution ΔH = −42.1 kcal/mol in comparison to the other inhibitor–enzyme complexes, explaining the weak calculated binding free energy (ΔG −24.8 kcal/mol).

As for the entropy results (ΔS) of the various drug-complexes, it should be noted that a more negative entropy

indicates greater restrictions of movement for the ligand in the active site, due to steric restrictions as well as stronger non-covalent inhibitor–enzyme interactions for certain parts of the inhibitor [113]. Such cases result in higher entropy penalties. The translational and rotational entropy contributions are in a close approximate range (−40 and −30 cal/mol K respectively) for all the inhibitors and only vary in the residual vibrational entropy ΔS_{vib} (Table 2).

The level of consistency attained by our theoretical method with the experimental data (Table 1) in this study suggests the computational model can be used to rationalize the different drugs–mutant PR binding interactions. However, the movement of the inhibitors closer to the Asp25/25′ residues during optimization, imply that omission of water molecules in the model is an over-simplification [42] and should be addressed in future studies to further improve the computational model.

AIM analysis

To characterize and classify the hydrogen bond formation between the QM region of the L38L↑N↑L PR and FDA approved drugs, the topological parameters using the AIM [53, 54] analysis was applied. The intermolecular HB for the charge density and its Laplacian ranges between 0.002–0.040 and 0.024–0.139 a.u, respectively [101, 102]. The negative value of $\nabla^2\rho(r)$ at BCP indicates a covalent interaction, while a positive $\nabla^2\rho(r)$ value depicts an electrostatic interaction [95, 103–105 The AIM topological indices computed at various BCPs for all the studied QM region of the L38L↑N↑L PR and FDA approved drug optimized at the DFT B3LYP/6-31G(d) are reported in Table 3

To classify the hydrogen bonds at BCP two topological values are usually applied [53, 101]. In all cases, the QM region of the L38L↑N↑L PR and FDA approved drugs form similar hydrogen bond interactions. The inhibitors exhibiting slightly better binding affinities with the L38L↑N↑L PR (Table 1), an average values of 0.075 and 0.129 a.u were observed for the electron density, $\rho(r)$ and Laplacian of electron density, $\nabla^2\rho(r)$ respectively. While inhibitors with weaker binding affinities (Table 1) showed average values of 0.062 a.u for the electron density, $\rho(r)$ and 0.158 a.u for Laplacian of electron density. Hence, these values indicate the presence of intermolecular hydrogen bond as per Bader and Popelier's criteria [53, 54]. It can be noticed that the better HIV PR binder, TPV has an average electron density value of 0.084 a.u and average Laplacian value of 0.064 a.u. Whereas, the weakest PR inhibitor, NFV has an electron density and Laplacian of electron density values of 0.027 and 0.070 a.u respectively from a single HB interaction (Table 3; Fig. 5). Also, the ellipticity value for TPV has an average of 0.066 a.u, while, NFV was computed to be 0.001 a.u, hence, TPV is observed to be more stable than NFV.

Table 3 The topological parameters in a.u, electron densities, $\rho(r)$, their Laplacians, $\nabla^2\rho(r)$, ellipticity (ε) at O···H BCPs and energetic parameters *V(r), G(r), H(r)* in kcal/mol between the QM region of the L38L↑N↑L PR and FDA approved drug at the B3LYP 6-31G(d) level of theory

Inhibitors	HB number	HB-interaction	Electron density $\rho(r)$	Laplacian $\nabla^2\rho(r)$	*V(r)*	*G(r)*	*H(r)*	Ellipticity (ε)
APV	HB1	$O_1\cdots HO_5$	0.0496	0.1310	0.0396	0.0362	0.0034	0.0252
	HB2	$O_5\cdots HO_4$	0.0606	0.1705	0.0537	0.0482	0.0055	0.0406
RTV	HB1	$O_1\cdots HO_5$	0.1486	−0.1486	0.2021	0.0825	0.1196	0.0127
	HB2	$O_5\cdots HO_4$	0.0960	0.1668	0.1029	0.0723	0.0306	0.0360
IDV	HB1	$0_2\cdots HO_5$	0.0602	0.1673	0.0518	0.0468	0.0050	0.0149
	HB2	$O_5\ldots HO_4$	0.0529	0.1524	0.0451	0.0416	0.0035	0.0440
LPV	HB1	$O_2\cdots HO_5$	0.0749	0.2219	0.0751	0.0653	0.0098	0.0210
	HB2	$O_5\cdots HO_4$	0.0558	0.1685	0.0506	0.0464	0.0042	0.0479
SQV	HB1	$O_1\cdots HO_5$	0.0449	0.1176	0.0353	0.0324	0.0030	0.0238
	HB2	$O_5\cdots HO_4$	0.0553	0.1579	0.0477	0.0436	0.0041	0.0402
DRV	HB1	$O_2\cdots HO_5$	0.0762	0.1808	0.0704	0.0578	0.0126	0.0162
	HB2	$O_5\cdots HO_4$	0.0587	0.1706	0.0520	0.0474	0.0047	0.0500
ATV	HB1	$O_2\cdots HO_5$	0.0858	0.1740	0.0830	0.0632	0.0198	0.0197
	HB2	$O_5\cdots HO_4$	0.0505	0.1499	0.0432	0.0403	0.0028	0.0446
TPV	HB1	$O_1\cdots HO_5$	0.1330	0.0284	0.1715	0.0893	0.0822	0.0173
	HB2	$O_5\cdots HO_4$	0.0341	0.0992	0.0281	0.0264	0.0016	0.0487
NFV	HB1	$O_2\cdots HO_5$	0.0266	0.0701	0.0213	0.0194	0.0019	0.0013

HIV protease inhibitors (HIV PIs) are ranked in terms of their binding free energies (ΔG)

HB represents the hydrogen bonds; where O_1 and O_2 corresponds to the oxygens of the un-protonated catalytic Asp (25); O_4 corresponds to the oxygen of the protonated catalytic Asp (25′); O_5 corresponds to the oxygen of the HIV PR inhibitors

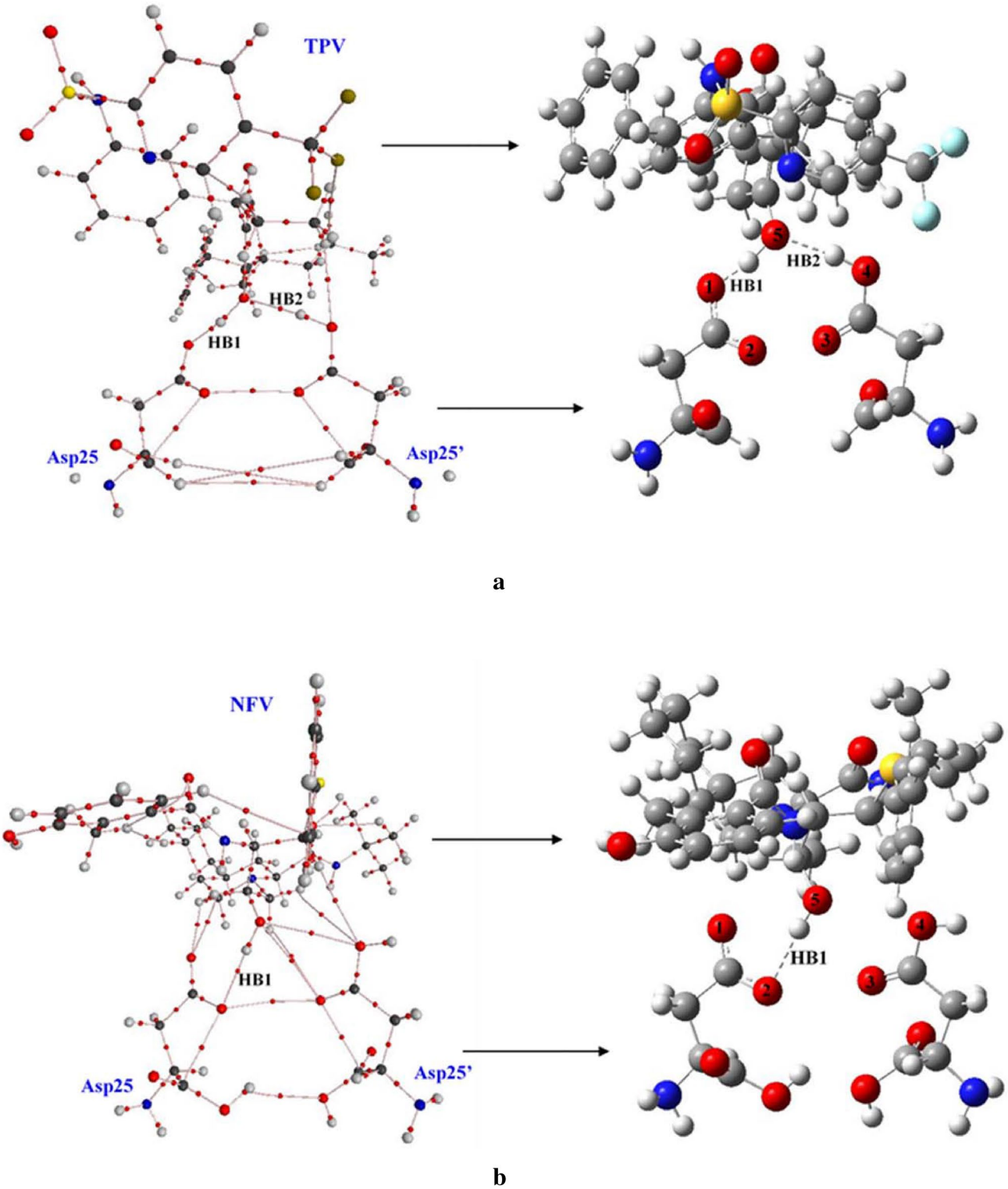

Fig. 5 **a** Molecular plot of the interaction in the TPV complexed with the catalytic Asp25/25′ of the enzyme. Small red dots correspond to the hydrogen interactions at the bond critical points (BCPs). **b** Molecular plot of the interaction in the NFV complexed with the catalytic Asp25/25′ of the enzyme. Small red dots correspond to the hydrogen interactions at the bond critical points (BCPs)

The Laplacian, $\nabla^2\rho(r)$ and the total energy density, H(r) values for all the hydrogen bond interactions are generally both positive, which indicates an electrostatic dominant interaction. Although, the HB1 in RTV is negative and positive respectively, and can be group as partially covalent-partially electrostatic bond [101, 114]. Figure 5 and S5 represent the intermolecular bond interaction at the BCP as red dots between the hydrogen atom donor and acceptor.

NBO analysis

The stabilization energies of the hydrogen bonds obtained at the DFT B3LYP/6-31G(d) calculation for all the investigated QM region of the L38L↑N↑L PR and FDA approved drug are analysed using the NBO theory and this is reported in Table 4. The hydrogen bond formation in the studied complexes indicates that a certain transfer of electronic charge occurs mostly from the bonding orbital (BD) to the unoccupied lone pair orbital (LP*). The intensive interaction of the hydrogen bond is directly proportional to the value of the $E^{(2)}$, i.e. the higher the value of $E^{(2)}$, the more stable the interaction [95, 101].

The results obtained from the NBO analysis demonstrate no significant difference in the second-order perturbation for all the investigated complexes. Large stabilization energy of 1.54 kcal/mol was observed as an average value for inhibitors with slightly better binding affinities (Table 1). Whereas, inhibitors with weaker binding affinities (Table 1) revealed a smaller reduction of 1.16 kcal/mol. On the hand, the better HIV PR binder, TPV has an average stabilization energy, $E^{(2)}$ of 2.43 kcal/mol and the weakest PR inhibitor, NFV has a stabilization energy, $E^{(2)}$ of 0.17 kcal/mol from a single HB interaction (Table 4). Hence the hydrogen bond strength is greater in TPV than in NFV.

Although, RTV exhibits high stabilization energy of 5.71 kcal/mol, this could be due to its existence of partially-covalent and partially-electrostatic bond (Table 3). These analyses are the same as the AIM study where the better binding inhibitors exhibits more stability than the weaker binders and, TPV exhibits more stability than NFV. It is important to emphasise that all the observed intermolecular hydrogen bond energy predicted using the NBO analyses correlates well with the above AIM discussion.

Table 4 Second-order perturbation $E^{(2)}$ in kcal/mol conforming to the most important charge transfer (donor→acceptor) at the B3LYP/6-31G(d) level of theory between the QM region of the L38L↑N↑L PR and FDA approved drugs

Inhibitors	HB number	Donor NBO (i)	Acceptor NBO (j)	$E^{(2)}$ kcal/mol
APV	HB1	BD(1)C–O_1	LP*(1)H_5	1.07
	HB2	BD(1)C–O_5	LP*(1)H_4	0.76
RTV	HB1	BD(1)C–O_1	LP*(1)H_5	5.71
	HB2	BD(1)C–O_5	LP*(1)H_4	0.96
IDV	HB1	BD(1)C–O_2	LP*(1)H_5	1.08
	HB2	BD(1)C–O_5	LP*(1)H_4	0.31
LPV	HB1	BD(1)C–O_2	LP*(1)H_5	1.53
	HB2	BD(1)C–O_5	LP*(1)H_4	0.88
SQV	HB1	BD(1)C–O_1	LP*(1)H_5	0.80
	HB2	BD(1)C–O_5	LP*(1)H_4	0.39
DRV	HB1	BD(1)C–O_2	LP*(1)H_5	1.86
	HB2	BD(1)C–O_5	LP*(1)H_4	0.72
ATV	HB1	BD(1)C–O_2	LP*(1)H_5	2.96
	HB2	BD(1)C–O_5	BD*(1) O_4–H_4	0.24
TPV	HB1	BD(1)C–O_1	LP*(1)HO_5	4.63
	HB2	BD(1)C–O_5	BD*(1) O_4–H_4	0.22
NFV	HB1	BD(1)C–O_2	BD*(1) O_5–H_5	0.17

HIV protease inhibitors (HIV PIs) are ranked in terms of their binding free energies (ΔG)

HB represents the hydrogen bonds. Where O_1 and O_2 corresponds to the oxygens of the un-protonated catalytic Asp (25); O_4 corresponds to the oxygen of the protonated catalytic Asp (25′); O_5 corresponds to the oxygen of the HIV PR inhibitors

Conclusion

This study involves the testing of a computational two-layered ONIOM computational model (QM:MM) to calculate the binding free energies of the nine FDA approved HIV-1 PIs. The calculated binding free energies for L38L↑N↑L HIV PR show a satisfactory trend with the experimental data with two exceptions. Two outliers, namely, TPV and NFV were observed, and analysis of hydrogen bond interactions and enthalpy contributions explained the observed anomalies. AIM analysis on the QM region of the L38L↑N↑L PR and FDA approved drugs justified the nature of the hydrogen bond interactions between the drugs and the active residues. The hydrogen bond interactions derived by AIM topological indices [$\rho(r)$, $\nabla^2\rho(r)$ and ε values] and the extent of charge transfer between the selected drugs and the active residues in close contact with drugs derived by second-order perturbation theory of NBO analysis can support the different binding affinities of the drugs against L38L↑N↑L PR. It is notable that our ONIOM [B3LYP/6-31G(d): AMBER] model can be further improved by the addition of water in the active pocket of the protease. Explicit water molecules should at least be treated at a semi-empirical level (PM6). These results will assist to systematically improve our computational model for the potential design of more potent HIV protease inhibitors.

Acknowledgements We thank the College of Health Sciences (CHS), Aspen Pharmacare, MRC and the NRF for financial support. We are also grateful to the CHPC (http://www.chpc.ac.za) and UKZN HPC cluster as our computational resources.

Compliance with ethical standards

Competing interests The authors declare that they have no competing interests.

References

1. Hensen C et al (2004) A combined QM/MM approach to protein-ligand interactions: polarization effects of the HIV-1 protease on selected high affinity inhibitors. J Med Chem 47(27):6673–6680
2. Shehu-Xhilaga M, Oelrichs R (2009) Basic HIV virology. In: HIV management in Australasia, Australian Society for HIV Medicine, Surry Hills, pp. 9–18
3. Brik A, Wong C-H (2003) HIV-1 protease: mechanism and drug discovery. Org Biomol Chem 1(1):5–14
4. Pearl LH, Taylor WR (1987) A structural model for the retroviral proteases. Nature 329(6137):351–354
5. Mildner AM et al (1994) The HIV-1 protease as enzyme and substrate: mutagenesis of autolysis sites and generation of a stable mutant with retained kinetic properties. Biochemistry 33(32):9405–9413
6. Braz AS et al (2012) Relation between flexibility and positively selected HIV-1 protease mutants against inhibitors. Proteins 80(12):2680–2691
7. Bonini C et al (2010) Synthesis of new thienyl ring containing HIV-1 protease inhibitors: promising preliminary pharmacological evaluation against recombinant HIV-1 proteases. J Med Chem 53(4):1451–1457
8. Mager PP (2001) The active site of HIV-1 protease. Med Res Rev 21(4):348–353
9. Clavel F, Mammano F (2010) Role of gag in HIV resistance to protease inhibitors. Viruses 2(7):1411–1426
10. Deeks SG et al (1997) HIV-1 protease inhibitors: a review for clinicians. Jama 277(2):145–153
11. Mitsuya H, Yarchoan R, Broder S (1990) Molecular targets for AIDS therapy. Science 249(4976):1533–1544
12. Katz RA, Skalka AM (1994) The retroviral enzymes. Annu Rev Biochem 63(1):133–173
13. Li D et al (2011) Strength of hydrogen bond network takes crucial roles in the dissociation process of inhibitors from the HIV-1 protease binding pocket. PLoS ONE 6(4):e19268
14. Kramer R et al (1986) HTLV-III gag protein is processed in yeast cells by the virus pol-protease. Science 231(4745):1580–1584
15. Huff JR (1991) HIV protease: a novel chemotherapeutic target for AIDS. J Med Chem 34(8):2305–2314
16. Hohlfeld K et al (2015) Disubstituted bis-THF moieties as new P2 ligands in nonpeptidal HIV-1 protease inhibitors (II). J Med Chem 58(9):4029–4038
17. Genoni A et al (2010) Computational study of the resistance shown by the subtype B/HIV-1 protease to currently known inhibitors. Biochemistry 49(19):4283–4295
18. Robbins AH et al (2010) Structure of the unbound form of HIV-1 subtype A protease: comparison with unbound forms of proteases from other HIV subtypes. Acta Crystallogr Sect D 66(3):233–242
19. Mosebi S et al (2008) Active-site mutations in the South African human immunodeficiency virus type 1 subtype C protease have a significant impact on clinical inhibitor binding: kinetic and thermodynamic study. J Virol 82(22):11476–11479
20. Verheyen J et al (2009) Prevalence of C-terminal gag cleavage site mutations in HIV from therapy-naive patients. J Infect 58(1):61–67
21. Hodge CN et al (1996) Improved cyclic urea inhibitors of the HIV-1 protease: synthesis, potency, resistance profile, human pharmacokinetics and X-ray crystal structure of DMP 450. Chem Biol 3(4):301–314
22. Brown D et al (2005) Antiviral activity of steric-block oligonucleotides targeting the HIV-1 trans-activation response and packaging signal stem-loop RNAs. Nucleosides Nucleotides Nucleic Acids 24(5–7):393–396
23. Nijhuis M et al (2007) A novel substrate-based HIV-1 protease inhibitor drug resistance mechanism. PLoS Med 4(1):e36
24. Lampejo T, Pillay D (2013) HIV virology, testing and monitoring. Medicine 41(8):420–424
25. Mao Y (2011) Dynamical basis for drug resistance of HIV-1 protease. BMC Struct Biol 11(1):1
26. Palmisano L, Vella S (2011) A brief history of antiretroviral therapy of HIV infection: success and challenges. Annali dell'Istituto superiore di sanitÃ 47(1):44–48
27. Liu Z et al (2013) Insights into the mechanism of drug resistance: X-ray structure analysis of multi-drug resistant HIV-1 protease ritonavir complex. Biochem Biophys Res Commun 431(2):232–238
28. Honarparvar B et al (2012) Pentacycloundecane-diol-based HIV-1 protease inhibitors: biological screening, 2D NMR, and molecular simulation studies. ChemMedChem 7(6):1009–1019
29. Makatini MM et al (2013) Synthesis, 2D-NMR and molecular modelling studies of pentacycloundecane lactam-peptides and peptoids as potential HIV-1 wild type C-SA protease inhibitors. J Enzyme Inhib Med Chem 28(1):78–88
30. Honarparvar B et al (2013) Integrated approach to structure-based enzymatic drug design: molecular modeling, spectroscopy, and experimental bioactivity. Chem Rev 114(1):493–537
31. Pawar SA et al (2012) Synthesis and molecular modelling studies of novel carbapeptide analogs for inhibition of HIV-1 protease. Eur J Med Chem 53:13–21
32. Pawar SA et al (2013) Linear and cyclic glycopeptide as HIV protease inhibitors. Eur J Med Chem 60:144–154
33. Karpoormath R et al (2012) Pentacycloundecane derived hydroxy acid peptides: a new class of irreversible non-scissile ether bridged type isoster as potential HIV-1 wild type C-SA protease inhibitors. Bioorg Chem 40:19–29
34. Makatini MM et al (2012) Synthesis, screening and computational investigation of pentacycloundecane-peptoids as potent CSA-HIV PR inhibitors. Eur J Med Chem 57:459–467
35. Karpoormath R et al (2013) Novel PCU cage diol peptides as potential targets against wild-type CSA HIV-1 protease: synthesis, biological screening and molecular modelling studies. Med Chem Res 22(8):3918–3933
36. Ahmed SM et al (2013) Comparison of the molecular dynamics and calculated binding free energies for nine FDA-approved HIV-1 PR drugs against subtype B and C-SA HIV PR. Chem Biol Drug Des 81(2):208–218
37. Lockhat HA et al (2015) Binding free energy calculations of nine FDA-approved protease inhibitors against HIV-1 subtype C I36T↑ T containing 100 amino acids per monomer. Chem Biol Drug Des 87:487–498
38. Ahmed SM et al (2014) The impact of active site mutations of South African HIV PR on drug resistance: insight from molecular dynamics simulations, binding free energy and per-residue footprints. Chem Biol Drug Des 83(4):472–481
39. Frisch A, Foresman J (1996) Exploring chemistry with electronic structure methods, vol 302. Gaussian Inc, Pittsburgh

40. Vreven T, Morokuma K (2000) On the application of the IMOMO (integrated molecular orbital + molecular orbital) method. J Comput Chem 21(16):1419–1432
41. Vreven T, Morokuma K (2006) Hybrid methods: Oniom (qm: mm) and qm/mm. Annu Rep Comput Chem **2**:35–51
42. Sanusi Z et al (2017) Investigation of the binding free energies of FDA approved drugs against subtype B and C-SA HIV PR: ONIOM approach. J Mol Graph Model 76:77–78
43. Maseko SB et al (2017) I36T↑ T mutation in South African subtype C (C-SA) HIV-1 protease significantly alters protease-drug interactions. Biol Chem. https://doi.org/10.1515/hsz-2017-0107
44. Fong P et al (2009) Assessment of QM/MM scoring functions for molecular docking to HIV-1 protease. J Chem Inform Model 49(4):913–924
45. Saen-oon S et al (2007) Insight into analysis of interactions of saquinavir with HIV-1 protease in comparison between the wild-type and G48V and G48V/L90M mutants based on QM and QM/MM calculations. J Mol Graph Model 26(4):720–727
46. Wittayanarakul K et al (2005) Insights into saquinavir resistance in the G48V HIV-1 protease: quantum calculations and molecular dynamic simulations. Biophys J 88(2):867–879
47. Shi S et al (2009) Molecular dynamics simulations on the role of protonation states in HIV-1 protease-indinavir complex. Acta Chim Sin 67:2791–2797
48. Tong Y et al (2009) Quantum calculation of protein solvation and protein–ligand binding free energy for hiv-1 protease/water complex. J Theor Comput Chem 8(06):1265–1279
49. Makatini MM (2011) Design, synthesis and screening of novel PCU-peptide/peptoid derived HIV protease inhibitors. University of KwaZulu-Natal, Westville
50. Smith R et al (1996) Ionization states of the catalytic residues in HIV-1 protease. Nat Struct Mol Biol 3(11):946–950
51. Honarparvar B et al (2015) Pentacycloundecane lactam vs lactone norstatine type protease HIV inhibitors: binding energy calculations and DFT study. J Biomed Sci 22(1):1–15
52. Maseko SB et al (2016) Purification and characterization of naturally occurring HIV-1 (South African subtype C) protease mutants from inclusion bodies. Protein Expr Purif 122:90–96
53. Bader RF (1990) Atoms in molecules. Wiley Online Library
54. Popelier P (2000) Atoms in molecules: an introduction. Harlow, Pearson Education
55. Reed AE, Curtiss LA, Weinhold F (1988) Intermolecular interactions from a natural bond orbital, donor-acceptor viewpoint. Chem Rev 88(6):899–926
56. Dahiya S, Gahlaut A, Kulharia M (2013) Comparative evaluation of commercially available homology modelling tools: a structural bioinformatics perspective. Drug Invent Today 5(3):207–211
57. Weber IT (1990) Evaluation of homology modeling of HIV protease. Proteins 7(2):172–184
58. Maghsoudi AH et al (2011) Homology modeling, docking, molecular dynamics simulation, and structural analyses of coxsakievirus B3 2A protease: an enzyme involved in the pathogenesis of inflammatory myocarditis. Int J Biol Macromol 49(4):487–492
59. Dhanavade MJ et al (2013) Homology modeling, molecular docking and MD simulation studies to investigate role of cysteine protease from *Xanthomonas campestris* in degradation of Aβ peptide. Comput Biol Med 43(12):2063–2070
60. Kohn W, Becke AD, Parr RG (1996) Density functional theory of electronic structure. J Phys Chem 100(31):12974–12980
61. Neumann R, Nobes RH, Handy NC (1996) Exchange functionals and potentials. Mol Phys 87(1):1–36
62. Becke AD (1993) Density-functional thermochemistry. III. The role of exact exchange. J Chem Phys 98(7):5648–5652
63. Lee C, Yang W, Parr RG (1988) Development of the Colle-Salvetti correlation-energy formula into a functional of the electron density. Phys Rev B 37(2):785–789
64. Hariharan PC, Pople JA (1973) The influence of polarization functions on molecular orbital hydrogenation energies. Theor Chim Acta 28(3):213–222
65. Rassolov VA et al (1998) 6-31G* basis set for atoms K through Zn. J Chem Phys 109(4):1223–1229
66. Case DA et al (2005) The Amber biomolecular simulation programs. J Comput Chem 26(16):1668–1688
67. Studio D (2013) 4.0 Tutorials. Receptor-Ligand Interaction. Accelrys Inc, San Diego
68. Laskowski RA, Swindells MB (2011) LigPlot+: multiple ligand–protein interaction diagrams for drug discovery. J Chem Inform Model 51(10):2778–2786
69. Biegler-König F, Schönbohm J (2002) Update of the AIM2000-Program for atoms in molecules. J Comput Chem 23(15):1489–1494
70. Kuiper BD et al (2015) The L33F darunavir resistance mutation acts as a molecular anchor reducing the flexibility of the HIV-1 protease 30 s and 80 s loops. Biochem Biophys Rep 2:160–165
71. Liu Z et al (2013) Crystallographic study of multi-drug resistant HIV-1 protease lopinavir complex: mechanism of drug recognition and resistance. Biochem Biophys Res Commun 437(2):199–204
72. Kuhnert M, Steuber H, Diederich WE (2014) Structural basis for HTLV-1 protease inhibition by the HIV-1 protease inhibitor indinavir. J Med Chem 57(14):6266–6272
73. Tie Y et al (2012) Critical differences in HIV-1 and HIV-2 protease specificity for clinical inhibitors. Protein Sci 21(3):339–350
74. Kožíšek M et al (2007) Molecular analysis of the HIV-1 resistance development: enzymatic activities, crystal structures, and thermodynamics of nelfinavir-resistant HIV protease mutants. J Mol Biol 374(4):1005–1016
75. Yedidi RS et al (2014) A conserved hydrogen-bonding network of P2 bis-tetrahydrofuran-containing HIV-1 protease inhibitors (PIs) with a protease active-site amino acid backbone aids in their activity against PI-resistant HIV. Antimicrob Agents Chemother 58(7):3679–3688
76. King NM et al (2012) Extreme entropy–enthalpy compensation in a drug-resistant variant of HIV-1 protease. ACS Chem Biol 7(9):1536–1546
77. DeLano WL (2002) The PyMOL molecular graphics system. DeLano Scientific, San Carlos
78. Cole JC et al (2005) Comparing protein–ligand docking programs is difficult. Proteins 60(3):325–332
79. Gohlke H, Hendlich M, Klebe G (2000) Knowledge-based scoring function to predict protein-ligand interactions. J Mol Biol 295(2):337–356
80. Kontoyianni M, McClellan LM, Sokol GS (2004) Evaluation of docking performance: comparative data on docking algorithms. J Med Chem 47(3):558–565
81. Li H, Robertson AD, Jensen JH (2005) Very fast empirical prediction and rationalization of protein pKa values. Proteins 61(4):704–721
82. Dolinsky TJ et al (2004) PDB2PQR: an automated pipeline for the setup of Poisson–Boltzmann electrostatics calculations. Nucleic Acids Res 32(suppl 2):W665-W667
83. Dennington R, Keith T, Millam J (2009) Semichem Inc, vol 5. Shawnee Mission KS, GaussView, Version
84. Vreven T et al (2006) Combining quantum mechanics methods with molecular mechanics methods in ONIOM. J Chem Theory Comput 2(3):815–826
85. Morokuma K (2002) New challenges in quantum chemistry: quests for accurate calculations for large molecular systems. Philos Trans Royal Soc Lond A 360(1795):1149–1164

86. Vreven T et al (2003) Geometry optimization with QM/MM, ONIOM, and other combined methods. I. Microiterations and constraints. J Comput Chem 24(6):760–769
87. Dapprich S et al (1999) A new ONIOM implementation in Gaussian98. Part I. The calculation of energies, gradients, vibrational frequencies and electric field derivatives. J Mol Struct (Thoechem) 461:1–21
88. Parr RG, Yang W (1984) Density functional approach to the frontier-electron theory of chemical reactivity. J Am Chem Soc 106(14):4049–4050
89. Johnson BG, Gill PM, Pople JA (1993) The performance of a family of density functional methods. J Chem Phys 98(7):5612–5626
90. Kapp J, Remko M, Schleyer PvR (1996) H_2XO and $(CH_3)_2XO$ compounds (X = C, Si, Ge, Sn, Pb): double bonds vs carbene-like structures can the metal compounds exist at all?. J Am Chem Soc 118(24):5745–5751
91. Remko M, Walsh OA, Richards WG (2001) Theoretical study of molecular structure, tautomerism, and geometrical isomerism of moxonidine: two-layered ONIOM calculations. J Phys Chem A 105(28):6926–6931
92. Frisch M et al (2009) 09, Revision D. 01, Gaussian, Inc., Wallingford, CT
93. Lundberg M et al (2010) Case studies of ONIOM (DFT: DFTB) and ONIOM (DFT: DFTB: MM) for enzymes and enzyme mimics. J Chem Theory Comput 6(4):1413–1427
94. Chung LW et al (2015) The ONIOM method and its applications. Chem Rev 115(12):5678–5796
95. Priya AM, Senthilkumar L, Kolandaivel P (2014) Hydrogen-bonded complexes of serotonin with methanol and ethanol: a DFT study. Struct Chem 25(1):139–157
96. Kosenkov D et al (2008) Tautomeric equilibrium, stability, and hydrogen bonding in 2′-deoxyguanosine monophosphate complexed with Mg^{2+}. J Phys Chem B 112(1):150–157
97. Senthilkumar L, Ghanty TK, Ghosh SK (2005) Electron density and energy decomposition analysis in hydrogen-bonded complexes of azabenzenes with water, acetamide, and thioacetamide. J Phys Chem A 109(33):7575–7582
98. Hao M-H (2006) Theoretical calculation of hydrogen-bonding strength for drug molecules. J Chem Theory Comput 2(3):863–872
99. Kotena ZM et al (2013) Hydrogen bonds in galactopyranoside and glucopyranoside: a density functional theory study. J Mol Model 19(2):589–599
100. Popelier P (1998) Characterization of a dihydrogen bond on the basis of the electron density. J Phys Chem A 102(10):1873–1878
101. Mosapour Kotena Z, Behjatmanesh–Ardakani R, Hashim R (2014) AIM and NBO analyses on hydrogen bonds formation in sugar-based surfactants (α/β-d-mannose and n-octyl-α/β-d-mannopyranoside): a density functional theory study. Liq Cryst 41(6):784–792
102. Popelier P, Bader R (1992) The existence of an intramolecular C·H·O hydrogen bond in creatine and carbamoyl sarcosine. Chem Phys Lett 189(6):542–548
103. Iwaoka M et al (2004) Nature of nonbonded Se⊙⊙⊙ O interactions characterized by 17O NMR spectroscopy and NBO and AIM analyses. J Am Chem Soc 126(16):5309–5317
104. Kheirjou S, Mehrpajouh S, Fattahi A (2013) Drastic influence of boron atom on the acidity of alcohol in both gas phase and solution phase, A DFT Study. J Theor Comput Chem 12(01):1250103
105. Kheirjou S, Fattahi A, Hashemi MM (2014) The intramolecular cation–π interaction of some aryl amines and its drastic influence on the basicity of them: AIM and NBO analysis. Comput Theor Chem 1036:51–60
106. Arnold WD, Oldfield E (2000) The chemical nature of hydrogen bonding in proteins via NMR: J-couplings, chemical shifts, and AIM theory. J Am Chem Soc 122(51):12835–12841
107. Lu Y-X et al (2007) Ab initio investigation of the complexes between bromobenzene and several electron donors: some insights into the magnitude and nature of halogen bonding interactions. J Phys Chem A 111(42):10781–10788
108. Matta CF, Boyd RJ (2007) An introduction to the quantum theory of atoms in molecules. In: The quantum theory of atoms molecules: from solid state to DNA and drug design. Wiley, Weinheim
109. Foster J, Weinhold F (1980) Natural hybrid orbitals. J Am Chem Soc 102(24):7211–7218
110. Weinhold F, Landis CR (2005) Valency and bonding: a natural bond orbital donor-acceptor perspective. Cambridge University Press, Cambridge
111. Majerz I (2012) Directionality of inter-and intramolecular OHO hydrogen bonds: DFT study followed by AIM and NBO analysis. J Phys Chem A 116(30):7992–8000
112. Behjatmanesh-Ardakani R (2015) NBO–NEDA, NPA, and QTAIM studies on the interactions between aza-, diaza-, and triaza-12-crown-4 (An-12-crown-4, n = 1, 2, 3) and Li+, Na+, and K + ions. Comput Theor Chem 1051:62–71
113. Ryde U (2014) A fundamental view of enthalpy–entropy compensation. MedChemComm 5(9):1324–1336
114. Nazari F, Doroodi Z (2010) The substitution effect on heavy versions of cyclobutadiene. Int J Quantum Chem 110(8):1514–1528